Inorganic Chemistry
Article

Inorg. Chem. **2010**, *49*, 3343–3350 **3343**
DOI: 10.1021/ic902409n

Phthalocyanine as a Chemically Inert, Redox-Active Ligand: Structural and Electronic Properties of a Nb(IV)-Oxo Complex Incorporating a Highly Reduced Phthalocyanine(4−) Anion

Edwin W. Y. Wong, Charles J. Walsby,* Tim Storr,* and Daniel B. Leznoff*

Department of Chemistry, Simon Fraser University, 8888 University Drive, Burnaby, BC, Canada V5A 1S6

Received December 4, 2009

This report describes the reduction of a niobium(V) phthalocyanine complex and investigation of the electronic structure of the resulting products. The reduction of $PcNbCl_3$ (Pc = phthalocyanine dianion) with 5.5 equiv of potassium graphite in 1,2-dimethoxyethane (DME) resulted in the isolation of $K_2PcNbO \cdot 5DME$ (**1a**). Addition of 18-crown-6 to **1a** gave $[K(18\text{-crown-}6)]_2(\mu\text{-DME})PcNbO$ (**1b**). Both **1a** and **1b** were structurally characterized by single-crystal X-ray diffraction analysis. In both complexes, the niobium center adopts a square pyramidal geometry and is coordinated by four basal Pc nitrogen atoms and an apical oxo ligand. Notably, the Pc ligand in **1a** is saddle-shaped, with significant bond length alternation, rather than flat with delocalized bonding. The production of ethylene during the reduction of $PcNbCl_3$, detected by gas chromatography/mass spectrometry (GC/MS), suggests that the oxo ligand likely results from double C−O bond activation of DME solvent. A combination of spectroscopic techniques and density functional theory (DFT) calculations were used to establish the electronic structure of **1a**. The close correspondence of the electronic absorption spectrum of **1a** to that of $[PcZn]^{2-}$ with a di-reduced Pc^{4-} ligand, indicates a similar electronic structure for the two complexes. Evaluation of the electronic transitions for **1a** and $[PcZn]^{2-}$ by time-dependent DFT calculations further suggests a similar electronic structure for both complexes, indicating that differences in symmetry between **1a** and $[PcZn]^{2-}$ do not significantly affect the nature of the electronic transitions. Electron paramagnetic resonance (EPR) spectroscopy of **1a** in solution at room temperature gave a 10-line spectrum, while frozen-solution X- and Q-band EPR spectra are consistent with powder-pattern spectra defined by uniaxial g and ^{93}Nb hyperfine tensors: these imply the presence of a d^1 Nb(IV) metal center. EPR and electron nuclear double resonance spectroscopy suggests that the spin density in **1a** is centered almost completely on the niobium, in agreement with the DFT calculations. These results illustrate the value of Pc as a chemically inert, redox-active ligand for stabilizing reactive metal centers.

Introduction

Ligand design lies at the heart of coordination chemistry,[1] and historically, ligands have been classified using terms such as spectator, innocent, or ancillary. In other words, these ligands were not expected to undergo chemical or oxidation state changes during a reaction, but were used to tune the overall reactivity of a complex. More recently, ligand cooperativity in catalysis has attracted significant interest, and elegant examples of chelate control[2] and substrate orientation via ligand-assisted molecular recognition events[3] have appeared in the literature. In addition, metal complexes with redox-active ligands, also known as non-innocent ligands, have been attracting great interest.[4] One reason for this is that redox-active ligands add another dimension of flexibility to

*To whom correspondence should be addressed. E-mail: dleznoff@sfu.ca (D.B.L.), tim_storr@sfu.ca (T.S.), cwalsby@sfu.ca (C.J.W.).

(1) *Comprehensive Coordination Chemistry II*; Lever, A. B. P., Eds.; Elsevier Ltd.: Oxford, 2004; Vol. *1*.

(2) Kalyani, D.; Deprez, N. R.; Desai, L. V.; Sanford, M. S. *J. Am. Chem. Soc*. **2005**, *127*, 7330.

(3) (a) Das, S.; Brudvig, G. W.; Crabtree, R. H. *Chem. Commun*. **2008**, 413. (b) Das, S.; Incarvito, C. D.; Crabtree, R. H.; Brudvig, G. W. *Science* **2006**, *312*, 1941.

(4) (a) Zweifel, T.; Naubron, J.-V.; Grützmacher, H. *Angew. Chem., Int. Ed*. **2009**, *48*, 559. (b) Nguyen, A. I.; Blackmore, K. J.; Carter, S. M.; Zarkesh, R. A.; Heyduk, A. F. *J. Am. Chem. Soc*. **2009**, *131*, 3307. (c) King, E. R.; Betley, T. A. *J. Am. Chem. Soc*. **2009**, *131*, 14374. (d) Zweifel, T.; Naubron, J.-V.; Buettner, T.; Ott, T.; Grützmacher, H. *Angew. Chem., Int. Ed*. **2008**, *47*, 3245. (e) Zarkesh, R. A.; Ziller, J. W.; Heyduk, A. F. *Angew. Chem., Int. Ed*. **2008**, *47*, 4715. (f) Scott, J.; Vidyaratne, I.; Korobkov, I.; Gambarotta, S.; Budzelaar, P. H. M. *Inorg. Chem*. **2008**, *47*, 896. (g) Ringenberg, M. R.; Kokatam, S. L.; Heiden, Z. M.; Rauchfuss, T. B. *J. Am. Chem. Soc*. **2008**, *130*, 788. (h) Adhikari, D.; Mossin, S.; Basuli, F.; Huffman, J. C.; Szilagyi, R. K.; Meyer, K.; Mindiola, D. J. *J. Am. Chem. Soc*. **2008**, *130*, 3676. (i) Vidyaratne, I.; Scott, J.; Gambarotta, S.; Budzelaar, P. H. M. *Inorg. Chem*. **2007**, *46*, 7040. (j) Ray, K.; Petrenko, T.; Wieghardt, K.; Neese, F. *Dalton Trans*. **2007**, 1552. (k) Knijnenburg, Q.; Gambarotta, S.; Budzelaar, P. H. M. *Dalton Trans*. **2006**, 5442. (l) Bart, S. C.; Chlopek, K.; Bill, E.; Bouwkamp, M. W.; Lobkovsky, E.; Neese, F.; Wieghardt, K.; Chirik, P. J. *J. Am. Chem. Soc*. **2006**, *128*, 13901. (m) Büttner, T.; Geier, J.; Frison, G.; Harmer, J.; Calle, C.; Schweiger, A.; Schönberg, H.; Grützmacher, H. *Science* **2005**, *307*, 235. (n) Pierpont, C. G. *Coord. Chem. Rev*. **2001**, *216*, 99. (o) Chaudhuri, P.; Wieghardt, K. *Prog. Inorg. Chem*. **2001**, *50*, 151. (p) Chaudhuri, P.; Verani, C. N.; Bill, E.; Bothe, E.; Weyhermuller, T.; Wieghardt, K. *J. Am. Chem. Soc*. **2001**, *123*, 2213.

Published on Web 03/12/2010

catalyst design. For instance, they have been used to design catalysts where the ligand oxidation state plays a key role in the catalytic activity of the metal complex,[5] and for extending the range of accessible oxidation states of a d^0 metal complex to allow for catalytic activity that would otherwise be impossible.[6]

Phthalocyanine (Pc) is a well-known redox-active ligand that normally possesses a −2 charge, but can exist in oxidation states ranging from Pc^0 to Pc^{6-}.[7] Pc has unique spectral properties and extremely high extinction coefficients; as a result of these properties, metallophthalocyanine (MPc) complexes have been synthesized for a broad range of applications (e.g., dyes and pigments, electronics, photodynamic cancer therapy).[8] In the area of catalysis, the bulk of the research with MPcs has been in the area of oxidation of organic compounds.[8,9] For example, an important industrial application is the oxidation of thiols by CoPc catalysts for removal of sulfur impurities in petroleum products.[9] On the other hand, there are a few reports[8,10] on using MPcs under heterogeneous, reducing conditions for small-molecule activation in Haber−Bosch- and Fischer−Tropsch-type reactions.[10]

In addition to their redox-active nature, Pc ligands are also considered to be chemically inert. MPc complexes, particularly the unsubstituted parent system, are renowned for their stability: many sublime at 350 °C[11] and are stable in strongly basic conditions.[12] This could enable them to resist activation by reactive metal centers.

We are interested in exploring the reactivity of complexes that combine the bond-activating ability of highly reduced, early transition metals with the chemical inertness and redox-active nature of Pc. Highly reduced, early transition metal complexes have been shown to cleave N_2,[13−16] E−E (E = pnictogen),[17] C−N,[18,19] C−O,[20] and C−C[21] bonds. Often, these highly reduced, reactive metal centers initiate undesirable reaction pathways involving activation of ancillary ligands or decomposition of the entire complex.[13,16,18,22,23] For example, reduction of a $SiMe_3$-substituted zirconium sandwich complex promotes activation of $SiMe_3$ and the formation of a cyclometalated zirconocene hydride.[23] Our initial efforts have been focused on studying the reactivity of reduced niobium phthalocyanine. The reduction of $PcNbCl_3$ in 1,2-dimethoxyethane (DME) results in a niobium phthalocyanine oxo complex where both the niobium center and the Pc ligand have been reduced. A combination of spectroscopic techniques and density functional theory (DFT) calculations was used to determine the electronic structure of this product, and the results are reported herein. The redox chemistry of MPcs is commonly investigated without isolating the species of interest,[7] and few MPcs with oxidized or reduced Pc ligands have ever been isolated and structurally characterized.[24] In particular, to our knowledge, the only structurally characterized MPcs with reduced Pc ligands are $AlPc^{3-}$,[25] $GePc^{4-}$,[26] and a reduced FePc[27] with an ambiguous electronic structure.

Results and Discussion

Synthesis and Structure. To access reduced PcNb systems, a suspension of $PcNbCl_3$[28] was reacted with 5.5 equiv of potassium graphite (KC_8) in DME, resulting in a dark purple mixture. Filtration and layering of hexanes onto the purple DME solution afforded extremely oxygen sensitive, intensely colored purple/green-gold dichroic crystals of $K_2PcNbO \cdot 5DME$ (**1a**) (Table 1).

The crystal structure of **1a** (Figure 1) reveals a monomeric, heterometallic compound consisting of a $[PcNbO]^{2-}$ anion and two K^+ cations solvated by five DME molecules. The niobium center has a square pyramidal geometry and is coordinated by the four basal Pc nitrogen atoms and an apical μ_3-oxo ligand. The average Nb−N bond distance of 2.120(4) Å is shorter than the

(5) Bouwkamp, M. W.; Bowman, A. C.; Lobkovsky, E.; Chirik, P. J. *J. Am. Chem. Soc.* **2006**, *128*, 13340.
(6) Blackmore, K. J.; Lal, N.; Ziller, J. W.; Heyduk, A. F. *J. Am. Chem. Soc.* **2008**, *130*, 2728.
(7) Stillman, M. J. Absorption and Magnetic Circular Dichroism Spectral Properties of Phthalocyanines. In *Phthalocyanines: Properties and Applications*; Leznoff, C. C., Lever, A. B. P., Eds.; VCH: New York, 1993; Vol. *3*, p 227.
(8) *The Porphyrin Handbook*; Kadish, K. M., Smith, K. M., Guilard, R., Eds.; Academic Press: San Diego, 2003; Vol. *19*.
(9) Chen, M. J.; Rathke, J. W. Phthalocyanines in Hydrocarbon Activation. In *Phthalocyanines: Properties and Applications*; Leznoff, C. C., Lever, A. B. P., Eds.; VCH: New York, 1996; Vol. *4*, p 183.
(10) Tamaru, K. *Catal. Rev. - Sci. Eng.* **1970**, *4*, 161.
(11) Stillman, M. J.; Nyokong, T. Absorption and Magnetic Circular Dichroism Spectral Properties of Phthalocyanines Part 1: Complexes of the Dianion, Pc(−2). In *Phthalocyanines: Properties and Applications*; Leznoff, C. C., Lever, A. B. P., Eds.; Wiley: New York, 1989; Vol. *1*, p 133.
(12) Byrne, G. T.; Linstead, R. P.; Lowe, A. R. *J. Chem. Soc.* **1934**, 1017.
(13) Fryzuk, M. D. *Acc. Chem. Res.* **2009**, *42*, 127.
(14) (a) Vidyaratne, I.; Crewdson, P.; Lefebvre, E.; Gambarotta, S. *Inorg. Chem.* **2007**, *46*, 8836. (b) Hirotsu, M.; Fontaine, P. P.; Epshteyn, A.; Zavalij, P. Y.; Sita, L. R. *J. Am. Chem. Soc.* **2007**, *129*, 9284.
(15) (a) Akagi, F.; Matsuo, T.; Kawaguchi, H. *Angew. Chem., Int. Ed.* **2007**, *46*, 8778. (b) Figueroa, J. S.; Piro, N. A.; Clough, C. R.; Cummins, C. C. *J. Am. Chem. Soc.* **2006**, *128*, 940. (c) Caselli, A.; Solari, E.; Scopelliti, R.; Floriani, C.; Re, N.; Rizzoli, C.; Chiesi-Villa, A. *J. Am. Chem. Soc.* **2000**, *122*, 3652. (d) Zanotti-Gerosa, A.; Solari, E.; Giannini, L.; Floriani, C.; Chiesi-Villa, A.; Rizzoli, C. *J. Am. Chem. Soc.* **1998**, *120*, 437.
(16) Kawaguchi, H.; Matsuo, T. *Angew. Chem., Int. Ed.* **2002**, *41*, 2792.
(17) (a) Seidel, W. W.; Summerscales, O. T.; Patrick, B. O.; Fryzuk, M. D. *Angew. Chem., Int. Ed.* **2009**, *48*, 115. (b) Cossairt, B. M.; Diawara, M.-C.; Cummins, C. C. *Science* **2009**, *323*, 602. (c) Figueroa, J. S.; Cummins, C. C. *Angew. Chem., Int. Ed.* **2004**, *43*, 984.
(18) (a) Tayebani, M.; Gambarotta, S.; Yap, G. P. A. *Angew. Chem., Int. Ed.* **1998**, *37*, 3002. (b) Tayebani, M.; Feghali, H.; Gambarotta, S.; Bensimon, C. *Organometallics* **1997**, *16*, 5084.
(19) (a) Kleckley, T. S.; Bennett, J. L.; Wolczanski, P. T.; Lobkovsky, E. B. *J. Am. Chem. Soc.* **1997**, *119*, 247. (b) Bonanno, J. B.; Henry, T. P.; Neithamer, D. R.; Wolczanski, P. T.; Lobkovsky, E. B. *J. Am. Chem. Soc.* **1996**, *118*, 5132.
(20) (a) Bradley, C. A.; Veiros, L. F.; Chirik, P. J. *Organometallics* **2007**, *26*, 3191. (b) Bradley, C. A.; Veiros, L. F.; Pun, D.; Lobkovsky, E.; Keresztes, I.; Chirik, P. J. *J. Am. Chem. Soc.* **2006**, *128*, 16600. (c) Proulx, G.; Bergman, R. G. *J. Am. Chem. Soc.* **1996**, *118*, 1981.
(21) (a) Agapie, T.; Diaconescu, P. L.; Mindiola, D. J.; Cummins, C. C. *Organometallics* **2002**, *21*, 1329. (b) Pellny, P.; Peulecke, N.; Burlakov, V. V.; Tillack, A.; Baumann, W.; Spannenberg, A.; Kempe, R.; Rosenthal, U. *Angew. Chem., Int. Ed. Engl.* **1997**, *36*, 2615.
(22) (a) Morello, L.; Ferreira, M. J.; Patrick, B. O.; Fryzuk, M. D. *Inorg. Chem.* **2008**, *47*, 1319. (b) Toomey, H. E.; Pun, D.; Veiros, L. F.; Chirik, P. J. *Organometallics* **2008**, *27*, 872. (c) Morello, L.; Yu, P.; Carmichael, C. D.; Patrick, B. O.; Fryzuk, M. D. *J. Am. Chem. Soc.* **2005**, *127*, 12796.
(23) Pun, D.; Lobkovsky, E.; Chirik, P. J. *J. Am. Chem. Soc.* **2008**, *130*, 6047.
(24) Engel, M. K. Single-Crystal Structures of Phthalocyanine Complexes and Related Macrocycles. In *Phthalocyanines: Structural Characterization*, Kadish, K. M., Smith, K. M., Guilard, R., Eds.; Academic Press: San Diego, 2003; Vol. *20*, p 1.
(25) Cissell, J. A.; Vaid, T. P.; Rheingold, A. L. *Inorg. Chem.* **2006**, *45*, 2367.
(26) Cissell, J. A.; Vaid, T. P.; Dipasquale, A. G.; Rheingold, A. L. *Inorg. Chem.* **2007**, *46*, 7713.
(27) Tahiri, M.; Doppelt, P.; Fischer, J.; Weiss, R. *Inorg. Chim. Acta* **1987**, *127*, L1.
(28) Cellucci, L.; Ercolani, C.; Lukes, P. J.; Chiesi-Villa, A.; Rizzoli, C. *J. Porphyrins Phthalocyanines* **1998**, *2*, 9.

Table 1. Crystallographic Data for **1a** and **1b**

	1a	**1b**
empirical formula	$C_{52}H_{66}O_{11}NbN_8K_2$	$C_{60}H_{74}O_{15}NbN_8K_2$
formula weight	1150.25	1318.39
crystal system	monoclinic	triclinic
space group	$P2_1/n$	$P1$
a (Å)	14.832(2)	11.1153(18)
b (Å)	20.841(3)	11.6215(19)
c (Å)	18.778(3)	13.624(2)
α (deg)	90	89.856(2)
β (deg)	106.131(2)	75.837(2)
γ (deg)	90	69.397(2)
V (Å^3)	5576.3(13)	1590.5(4)
Z	4	1
T (K)	150	293
ρ_{calcd} (g/cm^3)	1.370	1.376
μ (mm^{-1})	0.429	0.390
reflections collected	13145	13862
significant reflections	6644	13595
R [$I > 2.5\sigma(I)$]	0.0543	0.0500
R_w [$I > 2.5\sigma(I)$]	0.0524	0.0567
goodness of fit	1.1739	1.0318

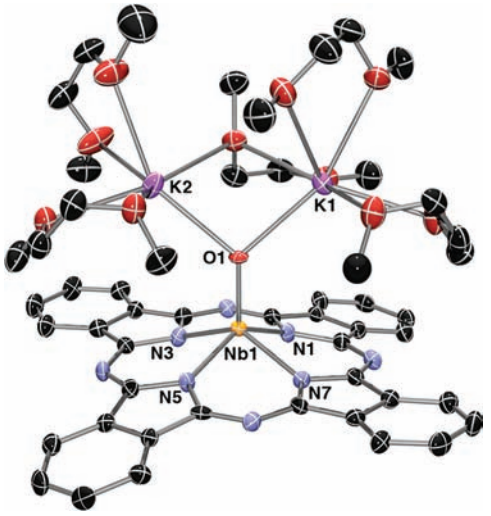

Figure 1. Molecular structure of **1a**. Thermal ellipsoids are set at 50% probability. Selected bond lengths [Å] and angles [deg]: Nb1−O1 1.761(3), Nb1−N1 2.112(5), Nb1−N3 2.127(4), Nb1−N5 2.108(4), Nb1−N7 2.132(4), K1−O1 2.713(4), K2−O1 2.704(4), N1−Nb1−N5 140.05(18), N3−Nb1−N7 138.82(17), Nb1−O1−K1 124.52(17), Nb1−O1−K2 124.77(17), K1−O1−K2 102.28(12). Nb1 to PcN_4 mean plane distance: 0.734 Å.

average distance reported for $PcNbCl_3$ (2.178(3) Å), and the niobium atom lies 0.734 Å above the PcN_4 plane, which is much lower than the 1.039(1) Å reported for $PcNbCl_3$.[28] These trends were also observed in the DFT geometry optimized structures for $PcNbCl_3$ and $[PcNbO]^{2-}$ (Supporting Information, Figures S1 and S2). The μ_3-oxo ligand connects the niobium to the two K^+ centers. Nb1, O1, K1, and K2 are not coplanar, and the oxo ligand takes on a distorted trigonal pyramidal geometry. The Nb−O bond distance of 1.761(3) Å is slightly longer than those reported for terminal Nb−O bonds,[29] consistent with cation−O interactions weakening the Nb−O bond.[30]

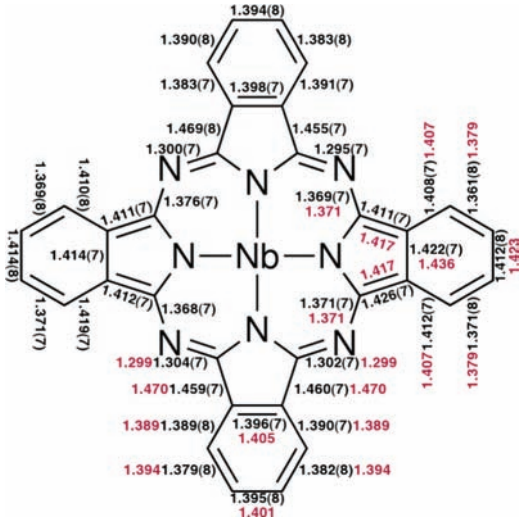

Figure 2. Demonstration of the bond length alternation within the Pc ligand of $[PcNbO]^{2-}$. Comparison of bond distances (Å) from the X-ray crystal structure of **1a** (black) and the DFT optimized structure (red). Symmetry equivalent bond lengths in the C_2-symmetric DFT optimized structure have been omitted.

The Pc ligand adopts a saddle-shape rather than the dome-shape observed for the $PcNbCl_3$ starting material. The dihedral angles between the C_8N_8 mean plane and the isoindole moieties in $NbPcCl_3$ are 14.1(1)°, 4.6(1)°, 9.0(1)°, and 8.3(1)°.[28] In **1a**, the Pc is curved along the axis containing the N1 and N5 isoindole moieties with dihedral angles of 10.54° and 12.92°, respectively, whereas, perpendicular to this axis, it is essentially flat. Furthermore, significant bond length alternation within the Pc ligand is observed around the C_8N_8 ring and in the benzo moieties along the flat axis of the ligand (Figure 2). Similar patterns of bond length alternation, which is not observed in $PcNbCl_3$, has been previously reported in di-reduced germanium Pc[26] and silicon and germanium porphyrin complexes.[31,32] This pattern was also reproduced in the DFT optimized structure of $[PcNbO]^{2-}$ (Figure 2). Bond length alternation of these di-reduced, 20 π-electron macrocycles has been attributed to their antiaromaticity.[26,31,32]

Addition of a slight excess of 18-crown-6 to **1a** in DME results in $[K(18\text{-crown-}6)]_2(\mu\text{-DME})PcNbO$ (**1b**) (Figure 3). X-ray quality crystals were obtained from the layering of hexanes onto a DME solution of **1b** (Table 1). The coordination geometry of the niobium center in **1b** remains the same as in **1a** while the μ_3-oxo becomes μ_2 and assumes a bent geometry. A second K^+-crown moiety is bridged to the oxo-bound K^+-crown ether via a μ-DME molecule. The Nb−O distance (1.724(3) Å) in **1b** is notably shorter than in **1a**. However, significant disorder of the $[PcNbO]^{2-}$ anion was observed in **1b** where approximately 18% of the anions exhibit the Nb=O moiety coordinated to the opposite face of the Pc ligand with the oxo bound to the K^+ on the adjacent molecule, making the Pc appear flatter[32] than in **1a** and limiting the accuracy of the $[PcNbO]^{2-}$ metrical parameters.

(29) (a) Figueroa, J. S.; Cummins, C. C. *J. Am. Chem. Soc.* **2003**, *125*, 4020. (b) Hubert-Pfalzgraf, L. G.; Tsunoda, M.; Leborgne, G. *J. Chem. Soc., Dalton Trans.* **1988**, 533. (c) Yu, J. S.; Fanwick, P. E.; Rothwell, I. P. *Acta Crystallogr., Sect. C: Cryst. Struct. Commun.* **1992**, *48*, 1759.
(30) Park, S. K.; Koo, S. M.; Lee, Y. E. *Polyhedron* **2000**, *19*, 1037.
(31) Cissell, J. A.; Vaid, T. P.; Rheingold, A. L. *J. Am. Chem. Soc.* **2005**, *127*, 12212.
(32) Cissell, J. A.; Vaid, T. P.; Yap, G. P. A. *J. Am. Chem. Soc.* **2007**, *129*, 7841.

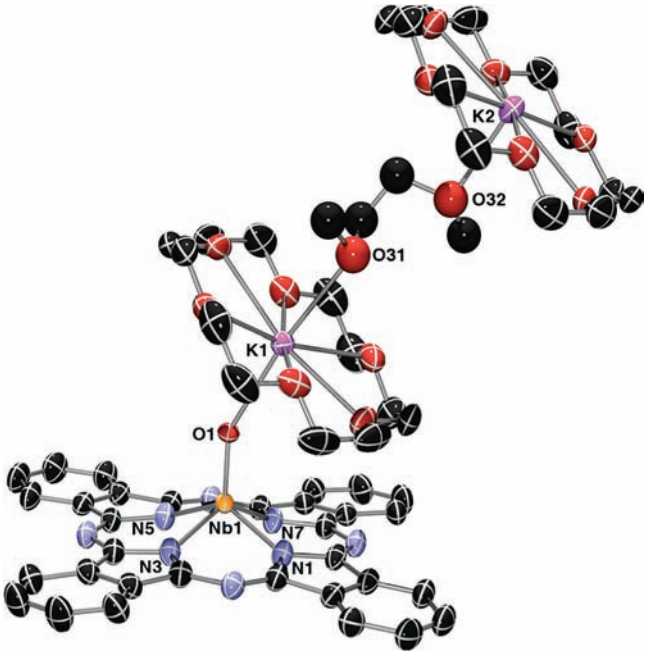

Figure 3. Molecular structure of **1b**. Thermal ellipsoids are set at 30% probability. Selected bond lengths [Å] and angles [deg]: Nb1−O1 1.724(3), Nb1−N1 2.133(3), Nb1−N3 2.163(3), Nb1−N5 2.128(3), Nb1−N7 2.130(3), K1−O1 2.656(3), K1−O31 2.848(8), K2−O32 2.657(9), N1−Nb1−N5 136.83(11), N3−Nb1−N7 135.86(11), Nb1−O1−K1 150.84(17). Nb1 to PcN_4 mean plane distance: 0.795 Å.

Identification of the Apical Ligand. A combination of experiments was performed to unambiguously confirm the identity of the apical ligand in **1a** as an oxide. Although the elemental analysis (C, H, N) of **1a** was inconclusive because of the variable, partial desolvation of DME, the more stable **1b** analyzed consistently for $[K(18\text{-crown-}6)]_2(\mu\text{-DME})PcNbO$.

To exclude the possibility of dinitrogen cleavage leading to nitride formation as has been previously observed with other Nb-containing species,[15,16,33] the synthesis of **1a** was performed under $^{15}N_2$, and the products were examined for ^{15}N incorporation. Electron paramagnetic resonance (EPR), electron nuclear double resonance (ENDOR), ^{15}N NMR and IR spectroscopy all failed to detect the ^{15}N label incorporated into any product, demonstrating that the apical ligand is not a nitride. Oxidation of **1a** with excess ferrocenium tetrafluoroborate and analysis of the resulting product using MALDI-TOF mass spectrometry verified the existence of a $[PcNbO]^{+\bullet}$ molecular ion (m/z = 621.70 Da). In addition, the calculated metrical parameters and electronic structure (vide infra) well match an oxo species. In summary, the spectroscopic and analytical data confirms that the apical ligand is an oxide.

Gambarotta and co-workers have reported that a low-valent uranium calix[4]tetrapyrrole complex cleaves the dinitrogen bond in DME solvent under a dinitrogen atmosphere, whereas the same complex activates the C−O bonds of DME under an argon atmosphere in the absence of dinitrogen.[34] In the case of **1a**, DME activation appears to be favored. The reduction of $PcNbCl_3$ in toluene under a dinitrogen atmosphere was performed to examine whether the system could be biased toward dinitrogen activation over solvent activation. Unfortunately, the resulting products could not be characterized because of their low solubility in toluene; further studies are in progress.

What is the source of the oxo ligand in **1a**? $NbCl_5$ is known to activate the C−O bonds of ethereal solvents such as tetrahydrofuran (THF) and DME,[35,36] and thus, it is possible that the starting material, $PcNbCl_3$, activated DME prior to reduction by KC_8. To test this mechanism, $PcNbCl_3$ was stirred in DME for 1 h (significantly longer than would normally occur during the synthesis of **1a**). Analysis of the reaction mixture by GC/MS found no C−O activation products, whereas analysis of a control mixture of $NbCl_5$ stirred in DME found several chlorinated DME derivatives, which are the expected C−O bond activation byproducts.[36] Hence, the starting $PcNbCl_3$ is not responsible for oxo incorporation in **1a**. However, DME is a likely source of the oxo ligand since, upon reduction of $PcNbCl_3$ to **1a**, ethylene was detected in the headspace of the reaction flask by GC/MS. In spite of this evidence, adventitious moisture or oxygen cannot be completely ruled out as the possible source of the oxo ligand.

UV−vis Spectroscopy. A series of spectroscopic data were examined to determine the electronic structure of the $[PcNbO]^{2-}$ system, in which both the niobium and Pc can exist in multiple oxidation states.[7,37] The UV−vis spectra of MPcs are dominated by the Pc ligand because the transitions associated with the ligand exhibit extremely large molar absorptivity coefficients ($> 10^5\ M^{-1}\cdot cm^{-1}$).[11] The position of λ_{max} for an MPc complex stays relatively constant across different metal centers,[11] whereas varying the charge on the Pc changes the spectrum significantly.[7] It is immediately apparent upon examination of the UV−vis spectra that λ_{max} of **1a/b** is dramatically blue-shifted in comparison to $PcNbCl_3$, and the Pc ligand no longer possesses the usual −2 charge (Figure 4 and Supporting Information, Figure S4). Indeed, the spectra of **1a/b** are similar to that of $[Pc^{4-}Zn^{II}]^{2-}$ (**2a**) and $[Pc^{4-}Mg^{II}]^{2-}$ (**2b**) bearing di-reduced Pc^{4-} ligands (Table 2); these have been previously recorded in DMF/piperidine and DMF solvent respectively, but not in DME. Electrochemically di-reduced zinc and magnesium porphyrazines also show similar spectra.[38]

To compare the spectra of **1a/b** and **2a** in the same solvent and thus rule out any potential spectral differences attributable to solvent, PcZn was reduced with 2 equiv of KC_8 in DME and the UV−vis spectrum obtained (Figure 4). In DME, the λ_{max} values of **1a/b** and **2a** are in even better agreement (Table 2). However, in solution, **2a/b** are planar and possess D_{2h} symmetry, whereas the out-of-plane coordination of niobium in **1a** reduces the symmetry to C_{2v}. We carried out time-dependent density

(33) Fryzuk, M. D.; Kozak, C. M.; Bowdridge, M. R.; Patrick, B. O.; Rettig, S. J. *J. Am. Chem. Soc.* **2002**, *124*, 8389.
(34) Korobkov, I.; Gambarotta, S.; Yap, G. P. A. *Angew. Chem., Int. Ed.* **2002**, *41*, 3433.
(35) (a) Marchetti, F.; Pampaloni, G.; Zacchini, S. *Chem. Commun.* **2008**, 3651. (b) Marchetti, F.; Pampaloni, G.; Zacchini, S. *Inorg. Chem.* **2008**, *47*, 365.
(36) Marchetti, F.; Pampaloni, G.; Zacchini, S. *Dalton Trans.* **2008**, 7026.
(37) Tau, P.; Nyokong, T. *J. Porphyrins Phthalocyanines* **2006**, *10*, 69.
(38) Donzello, M. P.; Ercolani, C.; Cai, X.; Kadish, K. M.; Ricciardi, G.; Rosa, A. *Inorg. Chem.* **2009**, *48*, 9890.
(39) Mack, J.; Stillman, M. J. *Inorg. Chem.* **1997**, *36*, 413.

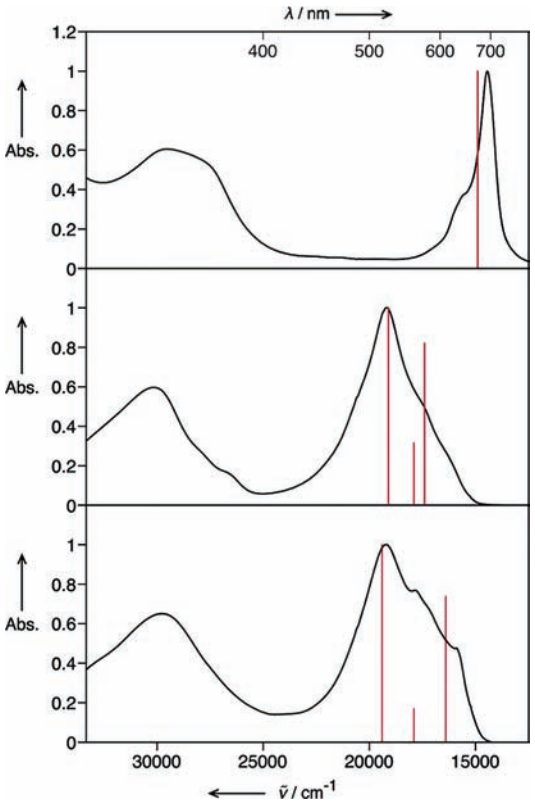

Figure 4. UV−vis absorption spectra of $PcNbCl_3$ (top) in $CHCl_3$, **1a** (middle) and **2a** (bottom) in DME. Calculated low energy transitions are shown in red.

Table 2. λ_{max} (nm) for PcNb, PcZn, and PcMg Complexes

compound[ref.]	solvent	λ_{max}	predicted λ_{max}[a]
$PcNbCl_3$	$CHCl_3$	692	671
1a	DME	521	523
1b	DME	522	
2a	DME	520	516
2a[39]	5:1 DMF/piperidine	540	
2b[7]	DMF	508	

[a] See Experimental Section for details.

functional theory (TD-DFT) calculations to probe the nature of the electronic transitions for $[PcNbO]^{2-}$, $[PcZn]^{2-}$, and the parent $PcNbCl_3$ to determine if this change in symmetry would be expected to induce significant changes in the UV−vis spectrum. The calculated λ_{max} (Table 2) are in good agreement with experimental values for the three species and indicate that there is no substantive impact on the λ_{max} of Pc^{4-} because of a global symmetry change in this case (523 nm vs 516 nm). The calculations predict that the transitions associated with λ_{max} for the three complexes are ligand-based (Supporting Information, Figures S5 to S7); with little contribution from the metal center. Thus, comparison of the energy and identity of the electronic transitions of **1a/b** and **2a**[40] indicates that the Pc unit exists in a doubly reduced Pc^{4-} state in these complexes.

EPR and ENDOR Spectroscopy. Complex **1a** exhibits strong, well-resolved EPR spectra when dissolved in DME, both at room temperature (Figure 5) and in frozen solution at 20 K (Figure 6). In the room-temperature spectrum, rapid tumbling essentially averages out anisotropic components of the Zeeman and hyperfine interactions, such that the spectrum is defined by a single g value, $g_{average} = 1.970$, and isotropic hyperfine coupling constant, $a = 165$ G. The distribution of line widths observed in this spectrum arises from a tumbling rate that is below the isotropic limit, in which case the molecular correlation time (τ_c) is not short enough to completely average out all anisotropic interactions at the microwave frequency of the experiment. Nonetheless, the spectrum is clearly in the fast-motion regime where the line positions are expected to be unchanged from the fully isotopic spectrum, and the lineshapes are still Lorentzian.[41] To ensure accurate determination of the $g_{average}$ and a values, the data were simulated using a polynomial expression for the line-width derived from Redfield theory: $1/T_2 = A + BM_I + CM_I^2$,[42] where the coefficients A, B, and C were determined by spectral simulation and the fwhm Lorentzian line-width in the frequency domain is given by $\delta B = 1/(\pi T_2)$ (Figure 5).[43,44] The observed average g value and ten-line hyperfine splitting pattern unequivocally identify a mononuclear niobium(IV) center ($4d^1$, $S = 1/2$; ^{93}Nb (100% isotopic abundance), $I = 9/2$), and are similar to

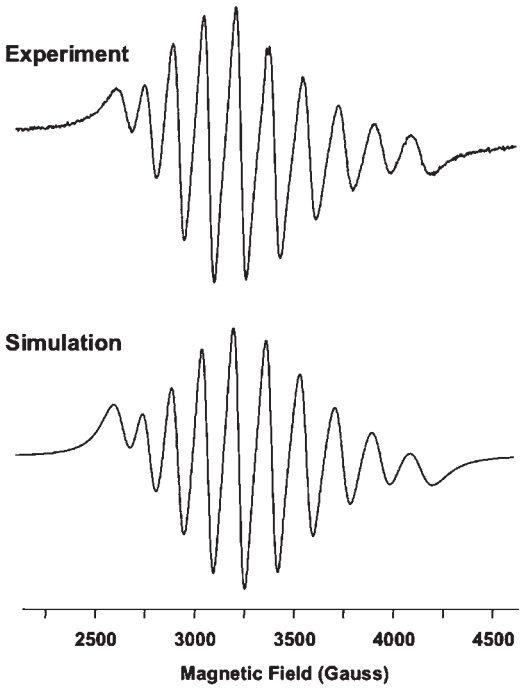

Figure 5. Room-temperature liquid-solution (DME) X-band EPR spectrum of **1a** and simulation. ***Experimental conditions:*** microwave frequency = 9.396 GHz, microwave power = 2.0 mW, modulation = 10.0 G, time constant = 10.24 ms, average of 20 20-s scans. ***Simulation parameters:*** $g = 1.970$, $a = 165$ G, Lorentzian line shapes. Linewidth modulation due to tumbling effects is fitted to the polynomial: $\delta B(G) = A + BM_I + CM_I^2$, to give $A = 50$ G, $B = -3$ G, $C = 3$ G.

(40) Mack, J.; Kobayashi, N.; Stillman, M. J. *J. Porphyrins Phthalocyanines* **2006**, *10*, 1219.

(41) Stoll, S.; Schweiger, A. *Biol. Magn. Reson.* **2007**, *27*, 299.

(42) Atherton, N. M. *Principles of electron spin resonance*; Ellis Horwood: Chichester, 1993.

(43) (a) Griffin, M.; Muys, A.; Noble, C. J.; Wang, D.; Eldershaw, C.; Gates, K. E.; Burrage, K.; Hanson, G. R. *Mol. Phys. Rep.* **1999**, *26*, 60. (b) Wang, D.; Hanson, G. R. *Appl. Magn. Reson.* **1996**, *11*, 401.

(44) Hanson, G. R.; Gates, K. E.; Noble, C. J.; Griffin, M.; Mitchell, A.; Benson, S. *J. Inorg. Biochem.* **2004**, *98*, 903.

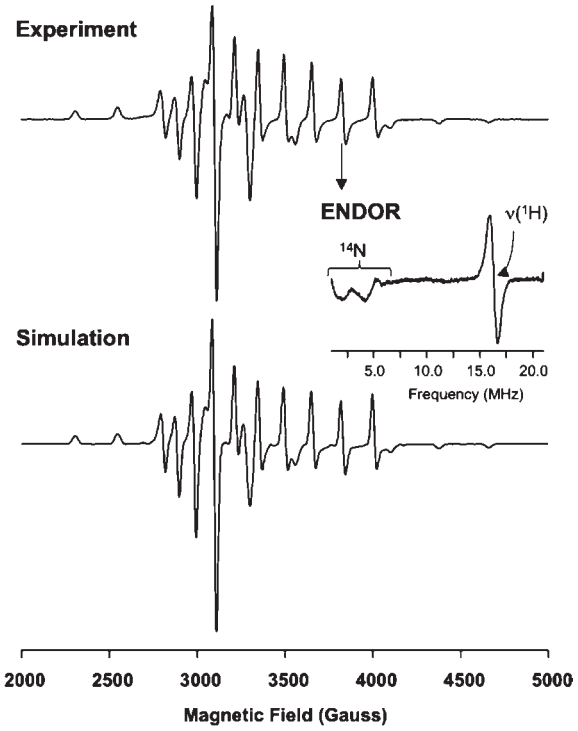

Figure 6. **Main figure:** Frozen-solution X-band EPR spectrum of **1a** in DME, and simulation. **Inset:** ENDOR spectrum at magnetic field = 3830.83 G (as indicated). ***EPR experimental conditions:*** microwave frequency = 9.472 GHz, microwave power = 6.3 mW, modulation = 4.0 G, time constant = 20.48 ms, temperature = 20 K, average of 2 40-s scans. ***ENDOR experimental conditions:*** microwave frequency = 9.471 GHz, microwave power = 6.3 mW, time constant = 20.48 ms, magnetic field = 3830.83 G, radio frequency power = 120 W, radio frequency modulation = 600 kHz, temperature = 20 K, average of 16 20-s scans. ***EPR simulation parameters:*** $g_\perp = 1.968$, $g_\parallel = 1.935$, $A_\perp = 132$ G, $A_\parallel = 262$ G, line width($\perp$) = 30 G, line width($\parallel$) = 46 G.

those reported previously for niobium(IV) porphyrin oxo complexes at room temperature (Table 3).

Measurements of the frozen-solution samples were conducted at two frequencies, X-band (9.5 GHz) (Figure 6) and Q-band (34 GHz) (Supporting Information, Figure S8), revealing powder-pattern EPR spectra defined by uniaxial g and ^{93}Nb hyperfine tensors, as anticipated based on the symmetry of the first-coordination sphere indicated by the crystal structure of **1a**. The spectra at both frequencies could be simulated precisely using a single set of parameters demonstrating accurate, unambiguous assignment of the EPR data. For comparison, Table 4 lists the g values and hyperfine coupling values of **1a** along with previously reported niobium(IV) porphyrin oxo species in frozen solutions. The close correspondence of these values with our measurements of **1a** demonstrate similar electronic ground states and ligand fields, as expected given the chemical and structural similarities of the ligands.

The uniaxial frozen-solution EPR spectrum of **1a**, which exhibits $g_\parallel < g_\perp$ ($g_\parallel = 1.935$, $g_\perp = 1.968$), is characteristic of a d_{xy}^1 ground state in an axially distorted octahedral ligand field,[46] in agreement with DFT calculations (Figure 7). Furthermore, analysis of the magnitudes of the isotropic and anisotropic components of the hyperfine

(45) Richard, P.; Guilard, R. *New J. Chem.* **1985**, *9*, 119.
(46) Richard, P.; Guilard, R. *J. Chem. Soc., Chem. Commun.* **1983**, 1454.

Table 3. Comparison of the Spin Hamiltonian Parameters for **1a** and Niobium(IV) Porphyrin Oxo Complexes in Solution[a]

compound[ref.]	solvent	T^b	g	a^c
1a	DME	298	1.970	165
(oep)NbO[45]	THF	298	1.967	181
(tpp)NbO[45]	THF	298	1.968	180

[a] oep = octaethylporphyrin; tpp = tetraphenylporphyrin. [b] In units of K. [c] In units of G.

Table 4. Comparison of the Spin Hamiltonian Parameters for **1a** and Niobium(IV) Porphyrin Oxo Complexes in Frozen Solution[a]

compound[ref.]	solvent	T^b	$g_\parallel$	$g_\perp$	$A_\parallel{}^c$	$A_\perp{}^c$
1a	DME	20	1.935	1.968	262	132
(tptp)NbO[45]	toluene	77	1.947	1.972	259	138
(oep)NbO[45]	toluene	77	1.934	1.972	272	143

[a] oep = octaethylporphyrin; tptp = tetra-*p*-tolylporphyrin. [b] In units of K. [c] In units of G.

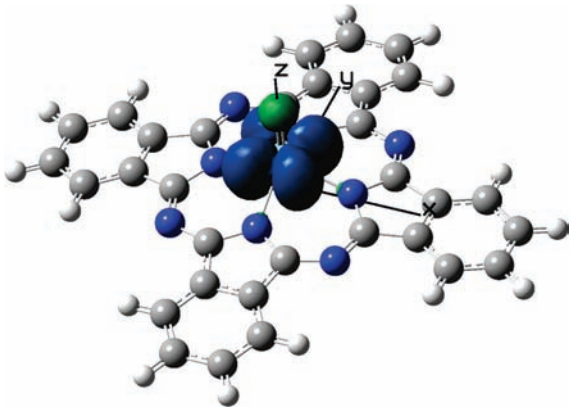

Figure 7. Calculated spin-density distribution for $[NbPcO]^{2-}$, showing the unpaired electron in the Nb $4d_{xy}$ orbital.

coupling ($A_\parallel = 262$, $A_\perp = 132$) reveals that approximately 93% of the total spin density is located in the $4d_{xy}$ orbital, with the remaining 7% in 5s, (see Supporting Information for details) again in agreement with the values obtained from DFT. Delocalization of the spin density onto the Pc ligand is minimal because the spin density resides in nonbonding $4d_{xy}$ and 5s orbitals of niobium.

Since the EPR and DFT studies indicated very little spin density on the Pc ligand of **1a** (Figure 7), electron nuclear double resonance (ENDOR) measurements were performed to characterize superhyperfine interactions, taking advantage of the order-of-magnitude greater resolution in hyperfine couplings available by this method as compared to conventional powder-pattern EPR. For a spin $I = 1/2$ nucleus, N, (e.g., ^{1}H) interacting with an $S = 1/2$ paramagnetic center, the ENDOR spectrum for a single molecular orientation is a doublet with line positions given by $\nu_\pm = |\nu_N \pm A/2|$, where ν_N is the Larmor frequency of the nucleus and A is the orientation-dependent hyperfine coupling, which allows identification of interacting nuclei in addition to determination of hyperfine couplings to the unpaired electron center. For $I > 1/2$, further splittings from quadrupolar interactions may be observed, but were not resolved in our measurements of ^{14}N ($I = 1$). ENDOR measurements of **1a** (Figure 6)

revealed superhyperfine couplings of $A(^{14}N) \leq 2$ G and $A(^{1}H) \leq 0.5$ G. In the latter case, no resolved splitting was observed, and the maximum possible ^{1}H hyperfine coupling value corresponds to the width of the resonant line observed. Observation of ^{14}N and ^{1}H resonances is as expected for the Pc ligand, but the very small hyperfine couplings observed demonstrate that remarkably little spin density is found outside the orbitals of the Nb metal center.

Conclusions

In summary, reduction of $PcNbCl_3$ in DME generates a niobium(IV) metal center coordinated by an oxo and a di-reduced Pc^{4-}. This work illustrates the potential of using Pc as a chemically inert, redox-active ligand for developing new catalysts. Chemical inertness allows Pc to stabilize reactive metal centers while its redox-active behavior opens up new possibilities for ligand participation in bond activation processes by using the ligand as an electron reservoir for catalytic reductions. With a MPc complex reported for nearly every transition metal, there is no shortage of candidates to study for their ability to facilitate useful chemical transformations.

Experimental Section

General Considerations. All manipulations were carried out under an atmosphere of dinitrogen in a MBraun Labmaster 130 glovebox or using standard Schlenk techniques unless otherwise stated.

Trichloro(phthalocyaninato)niobium(V)[28] and potassium graphite[47] were prepared according to literature procedures. Hexanes was dried over sodium wire and distilled under a nitrogen atmosphere, 1,2-dimethoxyethane (Certified, Fisher) was distilled under a nitrogen atmosphere from a purple solution of sodium benzophenone ketyl, and 1-chloronaphthalene (Technical, Aldrich) was vacuum distilled from CaH_2 prior to use. 18-Crown-6 (Puriss, Fluka) was dried overnight under vacuum. $^{15}N_2$ was purchased from Cambridge Isotope Laboratories in a 1 L break-seal flask. Upon delivery, a Teflon stir bar was placed in the neck of the flask above the break-seal and Kontes PTFE plug; a HI-VAC valve was joined to the flask. All other reagents were obtained from commercial sources and used as received.

NMR spectra were collected on a Bruker AVANCE II digital NMR spectrometer with a 5 mm QNP cryoprobe operating at 600 MHz for ^{1}H spectra.

UV−vis spectra were recorded on a Hewlett-Packard 8453 photodiode array spectrophotometer in a 0.1 cm quartz cell equipped with a Kontes PTFE plug, HI-VAC valve.

Infrared spectra were recorded on a Thermo Nicolet Nexus 670 FT-IR spectrometer. IR samples were prepared in a glovebox by drop-casting from a DME solution of the sample onto a calcium fluoride plate; a thin ring of grease was applied to the perimeter of the plate, sandwiched with a second calcium fluoride plate, and removed from the glovebox. Samples prepared in this fashion remained viable for at least 15 min.

Elemental analyses (C, H, N) were performed by Mr. Farzad Haftbaradaran at Simon Fraser University on a Carlo Erba EA 1110 CHN elemental analyzer. Samples for elemental analyses were loaded into pre-weighed tin capsules inside a glovebox, sealed by crimping the capsules with tweezers, removed from the glovebox, weighed, and promptly loaded into the analyzer.

Analysis of reaction mixtures of $NbCl_5$ or $PcNbCl_3$ in DME by GC/MS was performed on a HP G1800A GCD Series Gas Chromatograph Electron Ionization Detector. Ethylene was detected by GC/MS on a Varian 4000 GC/MS equipped with a FactorFour VF-5 ms column (0.25 mm × 0.25 μm × 30 m).

MALDI-TOF mass spectra were recorded on a PerSeptive Biosystems Voyager DE BioSpectrometry Workstation. Analyte solutions were prepared in $CHCl_3$ without a matrix.

EPR and ENDOR Spectroscopy. All EPR and ENDOR spectra were collected using a Bruker EMXplus spectrometer operating with either a premiumX X-band (~9.5 GHz) or a premiumQ Q-band (~34 GHz) microwave bridge. Low-temperature measurements of frozen solutions used a Bruker helium temperature-control system and continuous flow cryostats. Samples for X-band measurements were placed in 4 mm outer-diameter sample tubes with sample volumes of ~300 μL, while Q-band samples used 1.2 mm tubes containing ~30 μL of sample. ENDOR experiments used a Bruker DICE ENDOR system with an EN 801 X-band resonator and 150 W Bruker radio-frequency amplifier. EPR spectra were simulated with the XSophe simulation package.[44]

Computational Methods. Geometry optimizations and single-point calculations were performed using the Gaussian 03 program (Revision C.02),[48] the B3LYP functional,[49] the LanL2DZ basis set (Nb, Zn),[50] and the TZVP basis set of Ahlrichs (C, H, N, O, Cl).[51] The intensities of the 30 lowest-energy electronic transitions were calculated by TD-DFT[52] with the same functional/basis set combination employed for the single-point calculations, and a polarized continuum model (PCM) for CH_2Cl_2 (dielectric $\varepsilon = 8.94$).[53]

Single Crystal X-ray Crystallographic Analysis. All single crystal X-ray crystallographic analysis was performed on a Bruker SMART diffractometer equipped with an APEX II CCD area detector fixed at a distance of 6.0 cm from the crystal and a Mo Kα fine focus sealed tube ($\lambda = 0.71073$ nm) operated at 1.5 kW (50 kV, 30 mA) and filtered with a graphite monochromator.

Suitable crystals were loaded into 0.5 mm thin-walled glass capillaries for X-ray diffraction (05-SG, Charles Supper Company) inside a glovebox, temporarily sealed with grease, removed from the glovebox, and promptly flame-sealed. Temperature was regulated using an Oxford Cryosystems Cryostream. Structures were solved using direct methods (SIR92) and refined by least-squares procedures in CRYSTALS.[54] DME molecules in both **1a** and **1b** were disordered and modeled accordingly (see CIF file for details). The Nb═O unit in **1b** was disordered, with an 82:18 occupancy of two molecules in a 180° relative orientation (see CIF file for further details). Diagrams of **1a/b** were generated by ORTEP-3 for Windows (v. 2.00)[55] and rendered using POV-Ray (v. 3.6.1).[56] For the disordered atoms in the diagrams of **1a/b**, only the atoms with the higher occupancy are shown.

Synthesis of $K_2PcNbO \cdot 5DME$ (1a). KC_8 (0.522 g, 3.86 mmol) was added to a dark blue-green suspension of $PcNbCl_3$ (0.500 g,

(47) Schwindt, M. A.; Lejon, T.; Hegedus, L. S. *Organometallics* **1990**, *9*, 2814.

(48) Frisch, M. J. et al. *Gaussian 03*, Revision C.02; Gaussian, Inc.: Wallingford, CT, 2004.

(49) Becke, A. D. *J. Chem. Phys.* **1993**, *98*, 5648.

(50) (a) Hay, P. J.; Wadt, W. R. *J. Chem. Phys.* **1985**, *82*, 299. (b) Hay, P. J.; Wadt, W. R. *J. Chem. Phys.* **1985**, *82*, 270.

(51) Schafer, A.; Horn, H.; Ahlrichs, R. *J. Chem. Phys.* **1992**, *97*, 2571.

(52) (a) Casida, M. E. In *Recent Advances in Density Functional Methods*; Chong, D. P., Ed.; World Scientific: Singapore, 1995; p 155. (b) Stratmann, R. E.; Scuseria, G. E.; Frisch, M. J. *J. Chem. Phys.* **1998**, *109*, 8218.

(53) (a) Barone, V.; Cossi, M.; Tomasi, J. *J. Chem. Phys.* **1997**, *107*, 3210. (b) Barone, V.; Cossi, M.; Tomasi, J. *J. Comput. Chem.* **1998**, *19*, 404. (c) Miertus, S.; Scrocco, E.; Tomasi, J. *Chem. Phys.* **1981**, *55*, 117. (d) Tomasi, J.; Mennucci, B.; Cances, E. *J. Mol. Struct.* **1999**, *464*, 211.

(54) Betteridge, P. W.; Carruthers, J. R.; Cooper, R. I.; Prout, K.; Watkin, D. J. *J. Appl. Crystallogr.* **2003**, *36*, 1487.

(55) Farrugia, L. J. *J. Appl. Crystallogr.* **1997**, *30*, 565.

(56) *Persistence of VisionTM Raytracer*, Version 3.6.1; Persistence of Vision Pty. Ltd.: Williamstown, Victoria, Australia, 2004.

0.702 mmol) in about 20 mL of DME at room temperature. A color change to dark red-purple occurred over several minutes. The reaction mixture was stirred overnight and filtered through a minimal amount of Celite. The dark red-purple filtrate was evaporated under vacuum, and dichroic purple/green-gold crystalline powder was collected. Yield: 0.364 g (45.1%). Anal. Calcd for $C_{32}H_{16}N_8K_2NbO(C_4H_{10}O_2)_{3.6}$: C, 54.42; H, 5.12; N, 10.94. Found: C, 54.33; H, 5.51; N, 11.27. Crystals suitable for X-ray analysis were obtained by layering hexanes over a solution of **1a**.

Synthesis of [K(18-crown-6)]$_2$(μ-DME)PcNbO (1b). 1a (0.100 g, 0.098 mmol) and 18-crown-6 (0.054 g, 0.204 mmol) were added to about 10 mL of DME resulting in a dark red-purple solution. The solution was stirred for 10 min and filtered through a minimal amount of Celite. Crystals suitable for X-ray analysis were obtained by layering hexanes over the filtered solution in a 1:1 ratio. Yield: 0.048 g (37.3%). Anal. Calcd for $C_{60}H_{74}N_8K_2NbO_{15}$: C, 54.66; H, 5.66; N, 8.50. Found: C, 54.83; H, 5.55; N, 8.54.

Oxidation of 1a. 1a (0.150 g, 0.146 mmol) and ferrocenium tetrafluoroborate (0.178 g, 0.652 mmol) were added to about 10 mL of DME and stirred, resulting in a dark red-purple solution. Over a period of 20 min, the solution changed from dark red-purple to dark blue and finally to dark green. The solution was left to stir overnight and then evaporated under vacuum. The residue was extracted with hexanes and filtered with a frit, and the yellow filtrate discarded. The remaining solid on the frit was washed with toluene, and then DME and the dark green product was collected. Yield: 0.114 g. MALDI-MS, m/z (no matrix): calcd. for $[NbPcO]^{+\cdot}$: 621.05; found, 621.70.

Reduction of PcZn. KC_8 (0.235 g, 1.74 mmol) was added to a dark blue suspension of PcZn (0.500 g, 0.865 mmol) in about 25 mL of DME at room temperature. An immediate color change to dark purple occurred. The reaction mixture was stirred for 48 h and filtered through a minimal amount of Celite and a UV−vis spectrum of the dark purple filtrate was recorded. Yield: 0.681 g.

Acknowledgment. We gratefully acknowledge financial support provided by the Natural Sciences and Engineering Research Council of Canada and Simon Fraser University and WestGrid for computational resources. We thank Dr. M. J. Katz for assistance with X-ray crystallography.

Supporting Information Available: Details of the orbital occupancy and spin density calculations, supporting figures, details of the calculated structures and electronic transitions of **1a**, **1b**, and **2a**, CIF files for **1a** and **1b** Q-band EPR data, and complete ref 48. This material is available free of charge via the Internet at http://pubs.acs.org.